CHEMISTRY OF MATERIALS

Article

pubs.acs.org/cm

$CuIn_xGa_{1-x}S_2$ Nanocrystals with Tunable Composition and Band Gap Synthesized via a Phosphine-Free and Scalable Procedure

Enrico Dilena,[†,∥] Yi Xie,[†,∥] Rosaria Brescia,[†] Mirko Prato,[†] Lorenzo Maserati,[†] Roman Krahne,[‡] Andrea Paolella,[†] Giovanni Bertoni,[†,§] Mauro Povia,[†] Iwan Moreels,[†] and Liberato Manna*[,†]

[†]Nanochemistry Department and [‡]Nanostructures Department, Istituto Italiano di Tecnologia, via Morego 30, IT-16163 Genova, Italy

[§]IMEM-CNR, Parco Area delle Scienze 37/A, IT-43124 Parma, Italy

Supporting Information

ABSTRACT: We report a phosphine-free colloidal synthesis of $CuIn_xGa_{1-x}S_2$ (CIGS) nanocrystals (NCs) by heating a mixture of metal salts, elemental sulfur, octadecene, and oleylamine. In contrast with the more commonly used hot injection, this procedure is highly suitable for large-scale NC production, which we tested by performing a gram-scale synthesis. The composition of the CIGS NCs could be tuned by varying the In and Ga precursor ratios, and the samples showed a composition-dependent band gap energy. The average particle size was scaled from 13 to 19 nm by increasing the reaction temperature from 230 to 270 °C. Two concomitant growth mechanisms took place: in one, covellite (CuS) NCs nucleated already at room temperature and then incorporated increasing amounts of In and Ga until they evolved into chalcopyrite CIGS NCs. In the second mechanism, CIGS NCs directly nucleated at intermediate temperatures. They were smaller than the NCs formed by the first mechanism, but richer in In and Ga. In the final sample, obtained by prolonged heating at 230−270 °C, all NCs were homogeneous in size and composition. Attempts to replace the native ligands on the surface of the NCs with sulfur ions (following literature procedures) resulted in only around 50% exchange. Films prepared using the partially ligand exchanged NCs exhibited good homogeneity and an ohmic dark conductivity and photoconductivity with a resistivity of about 50 Ω·cm.

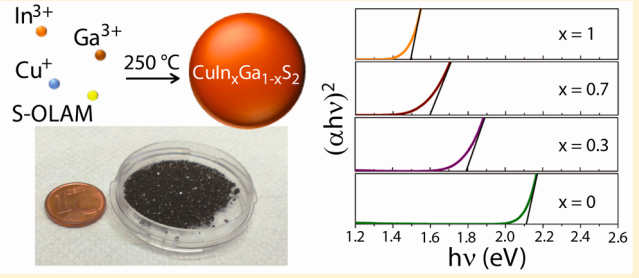

KEYWORDS: *nanocrystals, covellite, CIGS, large-scale synthesis, photovoltaics*

1. INTRODUCTION

There is an urgent need for sustainable energy sources, and large efforts are being directed at the efficient and cost-effective utilization of solar energy. Nowadays, the fabrication of photovoltaic absorber layers can be achieved by various means, including vacuum techniques (coevaporation,[1,2] sputtering,[3,4] field-assisted simultaneous synthesis and transfer (FASST)[5]), nonvacuum techniques (for example, electrodeposition,[3] sol−gel followed by chalcogenization,[6] dissolution of semiconductor components in hydrazine followed by deposition and thermal annealing[7,8]), and mixed approaches (such as FASST associated with liquid precursors).[9] An emerging low-cost strategy among the nonvacuum techniques is based on the deposition of inks of colloidal semiconductor nanocrystals (NCs) on a substrate using techniques such as spin-coating, dip-coating, doctor-blading, and ink-printing,[10−14] followed by thermal processing (and eventually postchalcogenization) of the NC layers to prepare absorber films of photovoltaic quality. Among the various NCs developed so far, those belonging to the II−VI and IV−VI classes of semiconductors have been intensively investigated in the past couple of decades.[15,16] However, considering the intrinsic toxicity of cadmium and lead, alternative classes of semiconductor NCs are considered more viable for photovoltaics. One important class is represented by Cu-based chalcogenides, such as Cu−In−S (CIS),[17,18] Cu−In−Se (CISe),[19−22] Cu−Ga−Se (CGSe),[21] Cu−In−Ga−S (CIGS),[23] Cu−In−Ga−Se (CIGSe),[10,19,21] Cu−In−Ga−S−Se (CIGSSe),[24] Cu−Sn−Se (CTSe),[25] Cu−Zn−Sn−S (CZTS),[26,27] and Cu−In−Zn−S (CIZS).[28]

To date, various synthesis approaches have been developed to prepare copper chalcogenides with composition, size, and shape control, such as the hot-injection approach[17,20,21] and the synthesis by direct heating of mixtures of precursors.[10,29] As an example, Wang et al.[23] synthesized wurtzite CIGS NCs with controllable shape and band gap by performing a hot injection of 1-dodecanethiol (1-DDT) and *tert*-dodecanethiol (t-DDT) in a solution containing acetylacetonate metal precursors, trioctylphosphine oxide (TOPO), and oleylamine (OLAM). Agrawal and co-workers synthesized CIS and CIGS NCs by a

Received: May 13, 2013
Revised: July 3, 2013
Published: July 8, 2013

   dx.doi.org/10.1021/cm401563u | *Chem. Mater.* 2013, 25, 3180−3187

Scheme 1. Sketch of the Two Concomitant Growth Mechanisms of CIGS NCs[a]

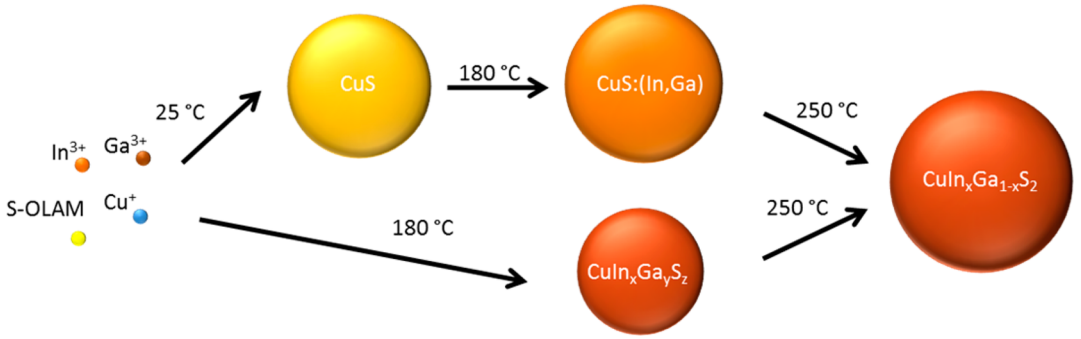

[a]In one case, covellite CuS seeds are formed first upon mixing of the chemicals at room temperature (25 °C). They subsequently evolve to intermediate CuS:(In,Ga) NCs (i.e., NCs incorporating In and Ga but still in the covellite phase) upon heating at 180 °C and to larger size, chalcopyrite $CuIn_xGa_{1-x}S_2$ NCs at 230−270 °C. In the second mechanism, residual precursors cause direct nucleation of chalcopyrite $CuIn_xGa_yS_z$ NCs, smaller in size than the NCs formed by the first mechanism, but richer in In and Ga. They also evolve into larger chalcopyrite $CuIn_xGa_{1-x}S_2$ NCs at 230−270 °C. In the final sample all NCs are homogenous in size and composition; i.e., there is no memory of the two alternative growth mechanisms.

hot injection of an OLAM-S precursor into an OLAM solution containing the corresponding metal chlorides at 225 °C.[24] Hot injection was also explored for the synthesis of Se-based ($CuGaSe_2$, $CuInSe_2$, and $Cu(InGa)Se_2$) NCs.[20,21] As an alternative to the procedures discussed above, ligand exchange with metal chalcogenide complexes (MCCs) was investigated recently for the synthesis of ternary and quaternary semiconductors.[19] Starting from Cu_2Se, CIGS-alloyed NCs were synthesized using $In_2Se_4^{2-}$ and gallium selenide MCCs, which served both as surface-stabilizing ligands and upon thermal annealing as reagents that generated ternary and quaternary phases.

The use of colloidal NC inks in the preparation of the active layer for photovoltaics requires manufacturing of large amounts of NC material, which calls for large-scale synthesis processes. The hot-injection route, being based on a fast injection of precursors, is unsuitable for large-scale synthesis, since up-scaling the small-volume, lab-based procedures typical of this approach is technically challenging. Improved results have been obtained via heating procedures that have been developed for the synthesis of S-based chalcogenide NCs.[18,29] Another method for a large- scale synthesis of quaternary ($CuIn_xGa_{1-x}S_2$) chalcopyrite NCs was developed by Sun et al., which relies on microwave decomposition of molecular single-source precursors.[30]

In the present work, we report a facile and up-scalable synthesis of chalcopyrite $CuIn_xGa_{1-x}S_2$ NCs by heating commercial metal salts (CuCl, $InCl_3$, and $GaCl_3$) in a sulfur solution containing octadecene (ODE) and OLAM. NCs with controlled composition ranging from $CuGaS_2$ to $CuInS_2$, through intermediate $CuIn_xGa_{1-x}S_2$ with tunable x, could be achieved by tailoring the precursor molar ratios. Also, the average particle size could be controlled from 13 to 19 nm by varying the reaction temperature (from 230 to 270 °C). We tracked the evolution of CIGS formation with increasing reaction temperature via transmission electron microscopy (TEM), X-ray diffraction (XRD), X-ray photoelectron spectroscopy (XPS), and optical absorption spectroscopy, which indicate that two parallel mechanisms are operative for the growth of the CIGS NCs during heating from 25 to 230−270 °C (Scheme 1): one is the diffusion of Ga and In ions into the CuS seeds that formed already at room temperature (RT). The other is the direct reaction of residual precursors at higher temperature. This second mechanism yields CIGS NCs with a smaller size but richer in In and Ga than those formed according to the first mechanism. However, all CIGS NCs reach homogeneous size and composition when the temperature is increased to 230−270 °C and the reaction is run for 30 min.

We additionally demonstrate the possibility of up-scaling for this method by performing a gram-scale synthesis of CIGS NCs. We also attempted to replace the native ligands on the surface of the NCs with sulfur ions following literature procedures. However, for the CIGS NCs developed by us, nuclear magnetic resonance spectroscopy indicated that only around 50% of the ligands could be replaced, and therefore, inks from these NCs are at present not entirely free from carbon. Surface treatment procedures certainly need further optimization for these NCs to reach complete ligand exchange. Films prepared from the partially ligand exchanged NCs were homogeneous (i.e., crack-free) and exhibited ohmic dark conductivity and photoconductivity, which suggests that the CIGS NCs might still be heavily doped.

2. METHODS

2.1. Chemicals. Copper chloride (CuCl; anhydrous beads, 99.99%), indium chloride ($InCl_3$; anhydrous, 99.999%), gallium chloride ($GaCl_3$; anhydrous beads, 99.999%), ammonium sulfide ($(NH_4)_2S$; 40−48 wt % aqueous solution), OLAM (>70%), ODE (90%), dimethylformamide (DMF; >99%), and dimethyl sulfoxide (DMSO; >99.9%) were purchased from Sigma-Aldrich. Elemental sulfur (99+%) was purchased from Strem Chemicals. Acetone (anhydrous, 99.8%) and toluene (anhydrous, 99.8%) were purchased from Carlo Erba Reagents. Deuterated chloroform ($CDCl_3$; 99.96% deuterated) and dimethyl sulfoxide (DMSO-d_6; 99.96% deuterated) were purchased from CortecNet. All chemicals were used as received without further purification.

2.2. Synthesis of CIGS NCs. In a typical small-scale synthesis, a 10 mL solution containing sulfur was prepared first by dissolving 0.035 g (1.1 mmol) of sulfur powder in 5 mL of OLAM and 5 mL of ODE and heating at 130 °C under vacuum for 30 min, followed by cooling to RT. Next, a mixture containing 0.050 g (0.5 mmol) of CuCl, 0.077 g (0.35 mmol) of $InCl_3$, and 0.026 g (0.15 mmol) of $GaCl_3$ was added to the previously prepared sulfur solution. The mixture was then placed under vacuum at RT for 90 min, followed by heating to a target temperature (typically 250 °C) under N_2 flow with a ramping rate of 5 °C/min, and was kept at this temperature for 30 min. The resulting product was cooled to RT and purified by precipitation with 20 mL of

dx.doi.org/10.1021/cm401563u | Chem. Mater. 2013, 25, 3180−3187

ethanol followed by centrifugation at 3000 rpm for 10 min. The supernatant, which contained byproducts and unreacted precursors, was then discarded, while the precipitate containing the NCs was redispersed in toluene. The NCs were purified again using the same procedure and finally redissolved in toluene and stored under a N_2 atmosphere.

For a gram-scale synthesis of CIGS NCs, 150 mL of a sulfur solution was first prepared by dissolving 0.528 g (16.5 mmol) of sulfur in 75 mL of OLAM and 75 mL of ODE. Then a mixture of 0.742 g (7.5 mmol) of CuCl, 1.161 g (5.25 mmol) of $InCl_3$, and 0.396 g (2.25 mmol) of $GaCl_3$ was added to a 250 mL flask containing the as-prepared sulfur solution, followed by degassing under vacuum for 90 min at RT. The system was then heated to 250 °C, and the reaction was kept at this temperature for 30 min, as described before. The resulting product was cooled to RT and cleaned twice using the same procedure as before, and finally the NCs were dispersed in toluene and stored under a N_2 atmosphere.

2.3. TEM Analysis. For conventional TEM investigations, the samples were prepared by drop-casting a NC dispersion on carbon-coated 200 mesh copper grids, and the images were acquired with a JEOL JEM-1011 microscope operating at 100 kV accelerating voltage. High-resolution TEM (HRTEM), scanning TEM (STEM) high-angle annular dark field (HAADF), and energy-dispersive X-ray spectroscopy (EDS) analyses were performed with a JEOL JEM-2200FS microscope operated at 200 kV and equipped with a CEOS image aberration corrector. The chemical composition was determined by EDS performed in the STEM-HAADF mode using a Bruker Quantax 400 system with a 60 mm^2 XFlash 5060 silicon drift detector (SDD). For HRTEM analyses NC solutions were drop-cast onto copper grids covered with an ultrathin amorphous carbon film, while for EDS analyses they were deposited onto carbon-coated aluminum grids and the measurements were carried out using a beryllium cup holder.

2.4. XPS Measurements. XPS was performed on a Kratos Axis Ultra DLD spectrometer using a monochromatic Al Kα source (15 kV, 20 mA). Wide scans were acquired at an analyzer pass energy of 160 eV. High-resolution narrow scans were performed at a constant pass energy of 20 eV and steps of 0.1 eV. The photoelectrons were detected at a takeoff angle $\Phi = 0°$ with respect to the surface normal. The pressure in the analysis chamber was maintained below 7×10^{-9} Torr for data acquisition. The data were converted to VAMAS format and processed using CasaXPS software, version 2.3.15. The binding energy (BE) scale was internally referenced to the C 1s peak (BE for C−C of 285 eV).

2.5. XRD Measurements. XRD measurements were recorded on a Smartlab 9 kW Rigaku diffractometer equipped with a copper rotating anode. The X-ray source was operated at 40 kV and 150 mA. A Göbel mirror was used to obtain a parallel beam. The specimen was prepared by drop-casting on a Si-miscut substrate. The measurements were performed using a $2\theta/\omega$ scan. The data analysis was performed using PDXL by Rigaku.

2.6. Ultraviolet−Visible−Near-Infrared (UV−Vis−NIR) Optical Absorption Measurements. UV−vis−NIR absorbance spectra were recorded with a UV−vis−NIR Cary 5000 (Varian) spectrophotometer in the wavelength range of 300−2000 nm. The NCs were dispersed in toluene for all measurements.

2.7. Elemental Analysis. The elemental analysis was carried out via inductively coupled plasma optical emission spectroscopy (ICP-OES) using an iCAP 6000 spectrometer. Dried samples were dissolved in HCl/HNO_3 (3:1, v/v) prior to the measurements.

2.8. Thermogravimetric Analysis (TGA). TGA was carried out using a thermogravimetric analyzer, Q500, from TA Instruments. TGA was used to estimate the weight fraction of the ligand shell surrounding the NCs. CIGS NCs were washed five times with toluene and ethanol to remove excess ligands in solution. About 20 mg of the precipitated sample was heated at 130 °C for 2 h to remove volatile components and excess unbound surfactants. Then, from RT, the sample was heated to 600 °C with a heating rate of 5 °C/min.

2.9. Ligand Exchange and Nuclear Magnetic Resonance (NMR) Spectroscopy. The as-prepared NCs were washed three times using toluene and absolute ethanol as the solvent and nonsolvent, respectively. The ligand exchange was performed using ammonium sulfide following a procedure similar to the one described by Nag et al.[31] In a nitrogen glovebox, a small-scale batch consisting of 20 mL of OLAM-capped CIGS NCs (CIGS_OLAM) in toluene (10 mg of NCs/mL) was prepared. We estimated, via simple geometric considerations, that the ligand shell of OLAM molecules around the NCs contributes about 7.5% to the total weight of the NCs (see Figure S10 in the Supporting Information), which was confirmed by TGA. Knowing the total amount of NCs in the solution, we added an amount of ammonium sulfide (dissolved in 10 mL of DMSO) that was, in terms of moles, 70 times larger than that of the OLAM ligand present in the sample. The resulting mixture was centrifuged and washed using DMSO to dissolve the NCs and toluene to precipitate them. This procedure was repeated two times to remove any residual free ammonium sulfide and OLAM. For NMR measurements, the ligand-exchanged CIGS (CIGS_S) precipitate was finally redispersed either in deuterated DMSO (for NMR measurements) or in DMF (for thin film-deposition and electrical characterization, see the next section). Equal amounts of OLAM-capped CIGS NCs were dried again and redispersed in deuterated chloroform. An appropriate volume of tetramethylsilane (TMS; about 1 μL) was added to these solutions as a concentration standard. Proton (^{1}H) NMR spectra were collected using a d_1 relaxation delay of 30 s to ensure full T_1 relaxation between the 90° excitation pulses, allowing a quantitative assessment of the spectra.[32] To relate the ligand densities before and after exchange, we compared the areas under the alkene resonances of OLAM, observed at around 5.5 ppm.

2.10. Thin-Film Deposition and Electrical Characterization. Interdigitated electrode structures were fabricated on Si/SiO_2 substrates by optical lithography and thermal evaporation of Ti/Au (thickness 5 nm/120 nm, respectively). The NC film was deposited by drop-casting a solution of S-capped NCs in DMF on the electrode devices under an inert atmosphere. To remove volatile residual organics, the films were heated at 180 °C in vacuum for 20 min prior to the measurements. The electrical transport measurements were performed with the sample placed under vacuum using a Keithley 2612 SourceMeter. For the photocurrent experiments the samples were illuminated with white light from a xenon lamp at 1 mW via an apertureless optical fiber positioned in proximity of the electrode structures (spot size ca. 100 μm).

3. RESULTS AND DISCUSSION

3.1. Small-Scale Synthesis of CIGS NCs. To monitor the evolution of the NCs during the reaction, aliquots were collected at different temperatures during heating. The aliquots collected at RT, 180 °C, and 250 °C contained a mixture of irregularly shaped nanoparticles with progressively increasing size (Figure 1a and Figure S1 of the Supporting Information). The XRD pattern of the aliquot collected at RT (Figure 1b) matched well with that of covellite CuS (hexagonal, space group $P6_3/mmc$, JCPDS 06-464), while the peak positions of the aliquot collected at 250 °C (Figure 1b) agreed with a chalcopyrite $CuIn_xGa_{1-x}S_2$ structure with $x \approx 0.7$ (tetragonal, space group $I\bar{4}2d$). Note that, as no pattern was reported in the JCPDS database for this exact composition, a pattern was calculated for this phase (see the Supporting Information for details). At intermediate temperatures, the diffraction features indicated a mixture of hexagonal covellite and chalcopyrite $CuIn_{0.7}Ga_{0.3}S_2$ (e.g., 180 °C, Figure 1b). The optical absorbance spectra (Figure 1c) of the aliquot samples collected at RT demonstrate a well-defined NIR absorption band, characteristic of a localized surface plasmon resonance in copper sulfide NCs.[33] For aliquots collected at higher temperatures, the intensity of the NIR absorption band was strongly reduced, confirming the decrease in the density of free carriers as the NCs evolved from CuS (metallic) to CIGS (a semiconductor). The formation of NCs in the covellite phase at RT was

dx.doi.org/10.1021/cm401563u | Chem. Mater. 2013, 25, 3180−3187

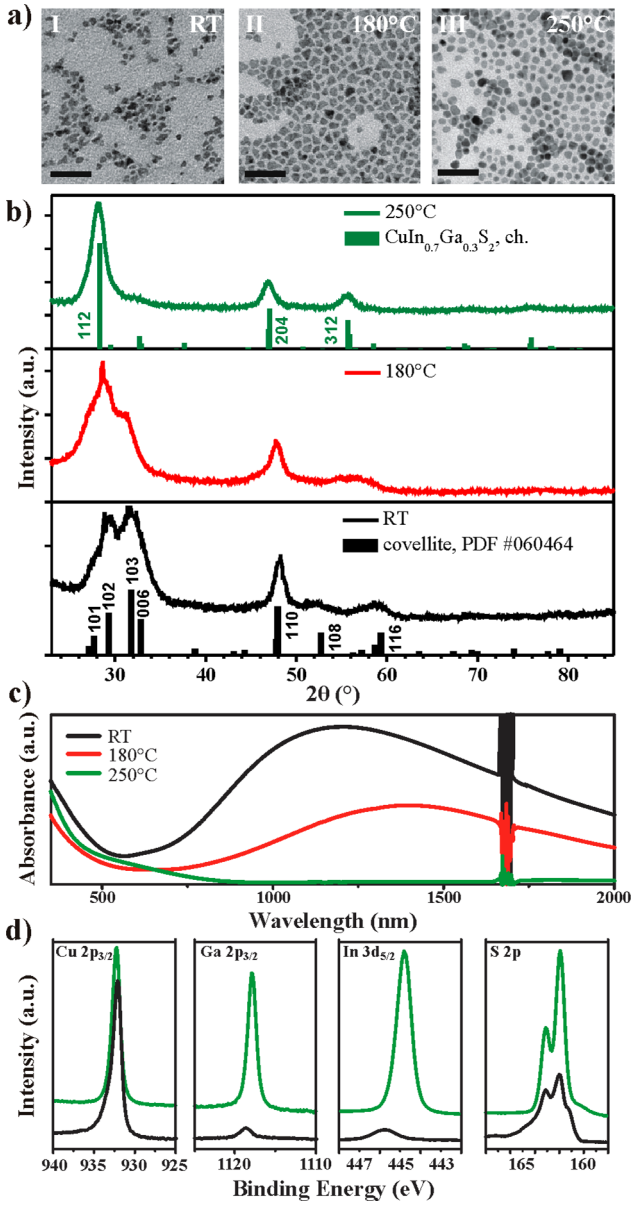

Figure 1. (a) TEM micrographs of aliquots collected at RT (I), 180 °C (II), and 250 °C (III) during heating. The scale bar is 50 nm. (b) XRD patterns of the three aliquots, compared to the reference patterns of covellite and chalcopyrite phases, and (c) corresponding absorbance spectra. (d) Comparison of high-resolution XPS on Cu $2p_{3/2}$, Ga $2p_{3/2}$, In $3d_{5/2}$, and S 2p peaks recorded on the RT aliquot (black lines) and on the sample obtained at 250 °C (green lines) after normalization to the Cu $2p_{3/2}$ intensity.

additionally confirmed by a control synthesis carried out at RT in the absence of the In and Ga precursors (see Figure S2 of the Supporting Information).

XPS analysis was performed on aliquots taken at the starting (RT) and final (250 °C) temperatures before the prolonged, 30 min heating to study the evolution of oxidation states and stoichiometries. The XPS results, after normalization to the intensity of the main Cu peak, are reported in Figure 1d and in Figures S3 and S4 of the Supporting Information. XPS survey spectra (Figure S3) indicate that the sample collected at 250 °C has a higher content of In and Ga with respect to the RT aliquot. High-resolution scans highlight even more the differences between the two samples (Figure 1d): an asymmetric Cu $2p_{3/2}$ peak and a multipeaked S 2p band recorded on the RT aliquot (see Figure S4 and related detailed discussion in the Supporting Information) are in good agreement with previous reports on CuS covellite,[34,35] thus supporting the XRD analysis. Low-intensity signals from Ga (Ga $2p_{3/2}$ at a BE of 1118.7 eV) and In (In $3d_{5/2}$ at a BE of 445.8 eV) were also present in BE ranges typical for Ga(III) and In(III),[36] which points to the presence of small amounts of complexes of Ga^{3+} and In^{3+} ions with surfactants as impurities in the final sample. XPS recorded on the sample obtained at 250 °C indicates that the oxidation numbers of copper and sulfur are +1 and −2, respectively. Concerning the Ga $2p_{3/2}$ and In $3d_{5/2}$ peaks, the increase in their intensity was also accompanied by a shift toward lower BE values (Figure 1d), which indicates a change in the chemical environment around those species. The peak positions were, however, still consistent with the presence of Ga(III) and In(III) and moreover in good agreement with the positions of Ga $2p_{3/2}$ and In $3d_{5/2}$ peaks found in CIGSe thin films.[37] Chemical compositions of the aliquots assessed by EDS analyses (Table S1, Supporting Information) further demonstrated the low Ga and In content (below the detection limit) and a slight excess in Cu (Cu/S atomic ratio 1.2) in the RT aliquot. A progressive increase in the relative In and Ga contents was observed for aliquots collected at higher temperatures (Table S1), in agreement with XPS analyses.

More details on the evolution of the morphologies, crystal structure, and optical spectra over the reaction temperature during the heating are provided in Figure S5 of the Supporting Information. As briefly mentioned above, the XRD patterns of the aliquots collected at intermediate temperatures (i.e., 180 and 200 °C) were a combination of the patterns of covellite CuS and chalcopyrite $CuIn_{0.7}Ga_{0.3}S_2$, suggesting that at this stage the samples consisted of a mixture of the two phases. These results are further confirmed by HRTEM analyses (Figure 2a–d). While in the initial NCs only the covellite structure was observed (Figure 2a), in the aliquot collected at 180 °C a mixture of covellite and chalcopyrite CIGS NCs was present (Figure 2b,c), with the latter structure observed in the smaller NCs. Moreover, at intermediate temperatures, a double population of particles was found, with a slightly higher In and Ga content and a lower Cu content in the smaller NCs (Figure 2f and inset; Table S2, Supporting Information).

It is clear that in our synthesis CuS NCs are formed first. The preferential reaction between Cu^+ and S precursors in the presence of In^{3+} and Ga^{3+} precursors was also observed by Chang et al.[38] and explained on the basis of the fact that the S precursor (in their case 1-dodecanethiol), being a soft Lewis base, reacted preferentially with a soft acid such as Cu^+, instead of hard acids such as In^{3+} and Ga^{3+}, leading to the formation of copper sulfide at the early stage of the synthesis. Similar arguments should apply in our case. Upon increasing the temperature, the as-formed covellite CuS nanoparticles are subjected to inward diffusion of In and Ga ions and a partial outward diffusion of Cu^+, with a negligible change in the crystal structure and an overall increase in size. The double population of NC sizes collected at 180 °C, with the smaller ones richer in indium and gallium than the larger CIGS NCs, suggests that at some stage there is a direct nucleation of CIGS NCs in a reaction environment with a reduced availability of Cu (see also Table S2, Supporting Information). The final sample however presented a homogeneous size distribution (with average size

dx.doi.org/10.1021/cm401563u | Chem. Mater. 2013, 25, 3180−3187

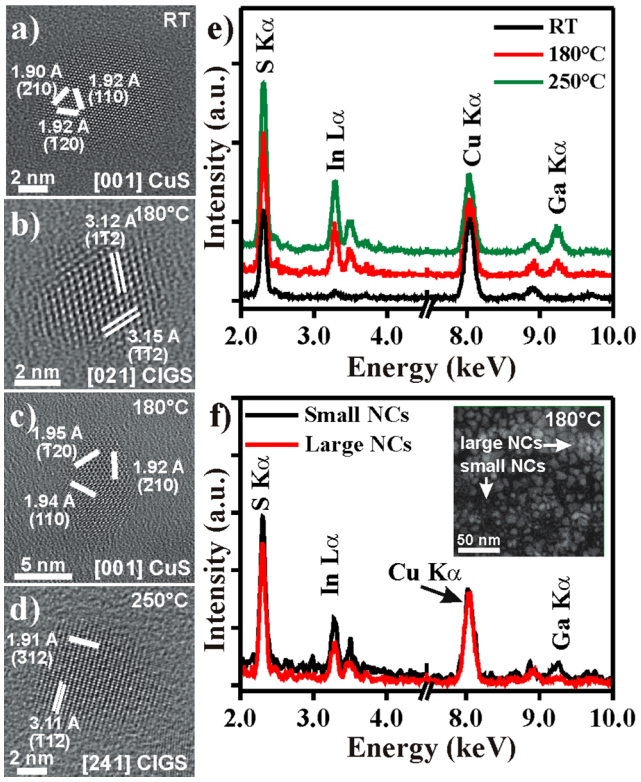

Figure 2. (a) HRTEM image of a typical particle from an aliquot collected at RT, characterized by the covellite structure. (b, c) HRTEM images of typical particles from an aliquot extracted at 180 °C during heating. Both chalcopyrite $CuIn_{0.7}Ga_{0.3}S_2$ (b) and covellite (c) structures are present at this reaction stage. (d) HRTEM image of a typical particle of chalcopyrite $CuIn_{0.7}Ga_{0.3}S_2$ from an aliquot extracted at 250 °C. (e) Overview EDS spectra recorded on the three aliquot samples (RT, 180 °C, and 250 °C), from which it is possible to observe the increase of S, In, and Ga with respect to Cu in aliquots collected at increasing reaction temperature. (f) Comparison of the EDS spectra collected from the two populations of NCs visible in STEM-HAADF images of the aliquot sample collected at 180 °C (in the inset). The smaller particles are richer in In and Ga with respect to the larger ones. The EDS spectra are normalized to the Cu Kα peak intensity.

larger than those of any intermediate aliquots) (Figure S6, Supporting Information).

The so-called seed-mediated growth in colloidal synthesis was already investigated by Hyeon et al., who performed thermal decomposition of a mixture containing Cu−oleate and In−oleate complexes in OLAM and DDT.[39] However, in that case chalcocite Cu_2S NCs instead of covellite CuS were formed first, which then evolved into heterostructured Cu_2S−CIS NCs. This was explained by considering that the hexagonal Cu_2S lattice matches well with the wurtzite $CuInS_2$ lattice, and consequently, it was possible to achieve epitaxial heterostructures by growing wurtzite $CuInS_2$ or ZnS on top of Cu_2S seeds.[38] Cui and co-workers further showed that it was possible for Cu_2S−$CuInS_2$ heterostructures to be converted to monophasic wurtzite $CuInS_2$ nanorods.[18] In our work, however, the initial covellite CuS NCs evolve to CIGS NCs with a chalcopyrite structure instead of the wurtzite structure. This can be explained on the basis of the lower thermodynamic stability of the wurtzite phase over the chalcopyrite one in our synthesis conditions.[23,40]

3.2. Composition, Band Gap, and Size Control over CIGS NCs.

By tailoring the precursor ratios, we were able to tune the In/Ga composition in the final NCs (see the quantification via EDS in Figure 3a and Table S3, Supporting

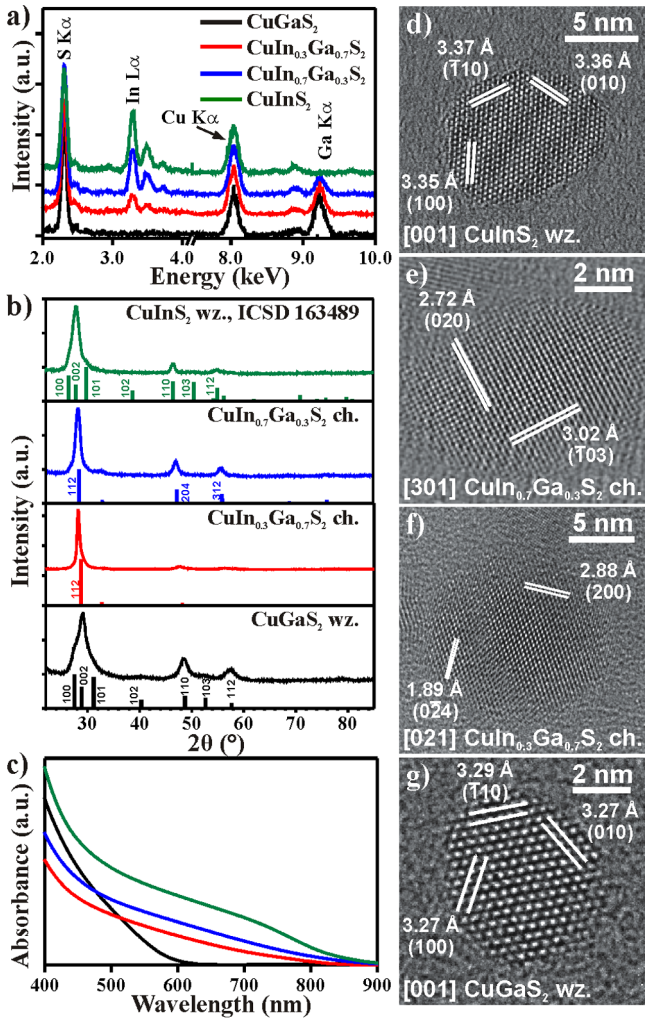

Figure 3. (a) EDS overview spectra, (b) XRD patterns, (c) optical absorbance spectra, and (d−g) HRTEM images of selected particles, obtained for samples synthesized by working at Cu:In:Ga precursor ratios of 1:0:1 (black, g), 1:0.3:0.7 (red, f), 1:0.7:0.3 (blue, e), and 1:1:0 (green, d). The EDS spectra are normalized to the peak intensity of the Cu Kα peak.

Information). The XRD pattern of the $CuInS_2$ NCs (Figure 3b) shows a good match with wurtzite $CuInS_2$.[40] Here, the (002) peak intensity is higher than it would be in a powderlike material, most likely because of [001] preferential orientation. This is supported by the observation that the NCs are thin [001]-oriented wurtzite platelets, as deduced by HRTEM analyses (Figure 3d). In a similar way, the $CuGaS_2$ NCs show a good match with preferentially [001]-oriented wurtzite (pattern calculated on the basis of parameters reported by Wang et al.),[23] as confirmed by HRTEM analyses (Figure 3g)). However, in both cases the presence of a minor portion of the chalcopyrite phase cannot be ruled out. The patterns of the two intermediate samples instead matched well with the calculated patterns for chalcopyrite $CuIn_{0.7}Ga_{0.3}S_2$ and $CuIn_{0.3}Ga_{0.7}S_2$ (more details about the pattern calculation are reported in the Supporting Information), respectively, in

dx.doi.org/10.1021/cm401563u | Chem. Mater. 2013, 25, 3180−3187

agreement with HRTEM analyses (Figure 3e,f). The optical absorption spectra of the NCs suspended in toluene showed a corresponding blue shift of the band edge as the Ga content increased (Figure 3c). Figure S7 (Supporting Information) reports a plot of $(\alpha h\nu)^2$ versus $h\nu$ (α = absorbance, h = Planck's constant, and ν = frequency), from which it is possible to extrapolate the slope near the absorption edge and extract the band gap energy.[23] The fits yielded 1.48, 1.57, 1.78, and 2.10 eV for wurtzite $CuInS_2$, chalcopyrite $CuIn_{0.7}Ga_{0.3}S_2$ and $CuIn_{0.3}Ga_{0.7}S_2$, and wurtzite $CuGaS_2$, respectively. The band gap values are close to those reported for wurtzite C(IG)S NCs of varying composition, ranging from 1.53 eV for CIS to 2.48 eV for CGS, as well as those of bulk chalcopyrite C(IG)S (quantum confinement effects can be neglected here due to the large NC dimensions).[10,23]

In addition to the control over the $CuIn_xGa_{1-x}S_2$ stoichiometry via the concentration of the initial metal salts, the reaction temperature was also a crucial parameter. Syntheses performed at different growth temperatures (from 230 to 270 °C) yielded CIGS NCs of different average sizes (Figure S8, Supporting Information). For example, by keeping all the other parameters unchanged (heating time 30 min and Cu:In:Ga:S precursor molar ratio equal to 1:0.8:0.4:2.2), the average particle size increased from 13 to 16 and 19 nm, respectively, when the synthesis temperature was increased from 230 to 250 and 270 °C. NC size distributions, as calculated from the TEM images, are reported in Figure S8e–g, demonstrating that a higher reaction temperature did not broaden the size dispersion.

3.3. Large-Scale Synthesis of CIGS NCs. The heating method presented here can provide a facile route for a large-scale synthesis of semiconductor NCs. To test the up-scaling, we increased the synthesis volume to 150 mL, which corresponds to a 15-fold increase of the volume compared to that in the syntheses discussed in the previous sections. Figure 4 summarizes the results of a typical gram-scale synthesis, performed in a 250 mL flask containing 75 mL of OLAM and 75 mL of ODE. The heating time at 250 °C was again 30 min, and the Cu:In:Ga precursor molar ratio was set at 1:0.7:0.3. The average diameter of the particles was 12 ± 2 nm (see the TEM image and corresponding size distribution in Figure 4a and inset). HRTEM and FFT of individual NCs (e.g., Figure 4b) and the XRD pattern collected on an NC thin film (Figure 4d) confirmed that the NCs have a chalcopyrite crystal structure and that no other phases or side products were formed in the reaction. STEM–EDS elemental maps of several NCs (Figure 4c) confirmed that S, Cu, Ga, and In were evenly distributed inside the NCs, with an average Cu:In:Ga:S molar ratio of 1.3:0.7:0.4:2 (Figure S9, Supporting Information). The atomic concentrations measured from several individual NCs (Table S4, Supporting Information) confirmed the homogeneous composition of the sample. On the basis of the absorbance spectra, the band gap energy determined by plotting $(\alpha h\nu)^2$ versus $h\nu$ was 1.59 eV (Figure 4e), in good agreement with the band gap of small-scale-synthesized CIGS NCs with the same composition (Figure S7, Supporting Information).

An important aspect of a large-scale synthesis of NCs is the synthesis yield. This was estimated from a comparison of the total weight of the product and that of the initial precursors. In calculating the yield, the contribution of the organic surfactants to the weight of the final product was estimated from TGA analysis and subsequently subtracted (Figure S10, Supporting

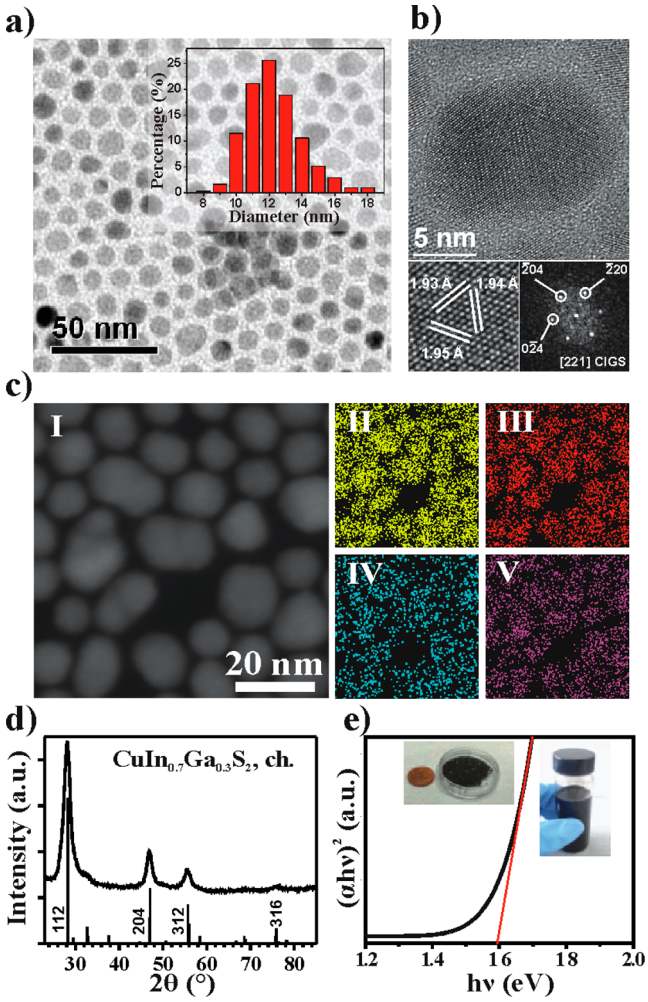

Figure 4. CIGS NCs prepared via a large-scale version of the synthesis. (a) TEM image of CIGS NCs. The inset provides the size distribution. (b) HRTEM image of a typical CIGS NC and corresponding FFT, showing the chalcopyrite $CuIn_{0.7}Ga_{0.3}S_2$ structure. (c) STEM-HAADF image of a group of CIGS NCs (I) and corresponding S (II), Cu (III), Ga (IV), and In (V) EDS elemental maps. (d) XRD pattern and (e) absorbance spectrum of CIGS NCs, with an extrapolation of the spectra (red line) to determine the band gap value. The insets in (e) are photographs of a solution of CIGS NCs in toluene (left) and of a dried powder of the same NCs (right).

Information), from which a synthesis yield of 90% was found. We can therefore conclude that the present synthesis approach can produce CIGS NCs in gram-scale amounts, while avoiding at the same time excessive loss of unreacted precursors, and with excellent control over the crystal phase, composition, band gap energy, and particle size.

3.4. Ligand Exchange and Electric Characterization. To develop inks of NCs that are free from carbon-containing stabilizers, the native OLAM ligands coating the NC surface, as a result of the use of OLAM in the synthesis, need to be exchanged. We used ammonium sulfide for the ligand exchange, which leaves the surface of the NCs passivated with S^{2-} anions,[31] and evaluated the exchange efficiency with quantitative ^1H NMR spectroscopy. This was done by comparing the relative area under the 5.5 ppm resonance arising from the alkene protons of the OLAM (Figure 5a,b). TMS, which yields a well-separated resonance at 0 ppm, was used as a concentration standard. The analysis of the spectra

dx.doi.org/10.1021/cm401563u | Chem. Mater. 2013, 25, 3180–3187

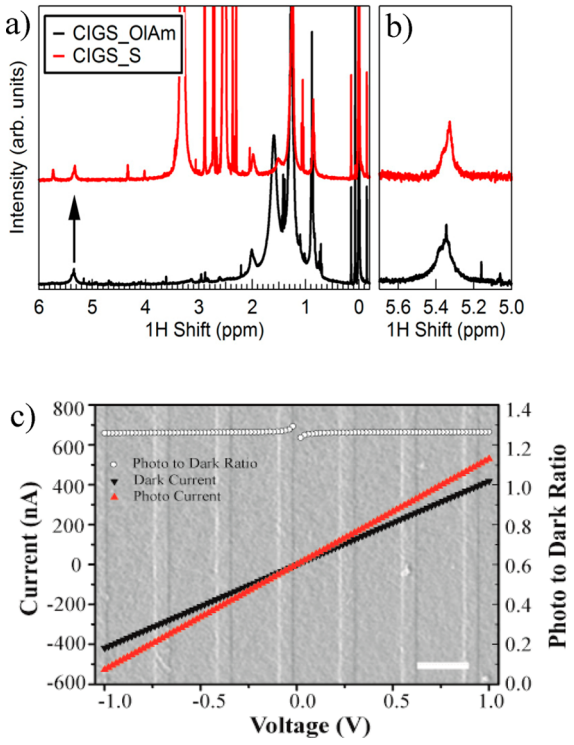

Figure 5. (a, b) Quantitative ^{1}H NMR spectrum before (bottom, CIGS_OLAM) and after (top, CIGS_S) ligand exchange. The TMS resonance at 0 ppm is used as a reference, and the area under the alkene resonance is compared (arrow) to assess the exchange efficiency. Minor (sharper) resonances are observed due to residual organic impurities. Additionally, strong resonances due to DMSO-d_6, residual nondeuterated DMSO, and possible traces of water are observed at 2.50, 2.54, and 3.31 ppm, respectively. (c) Current–voltage curves recorded from CIGS nanocrystal films at RT in the dark (black) and under white light illumination (red), plotted together with the dark current to photocurrent ratio (empty circles). The SEM image in the background shows the high-quality film that was obtained from $(NH_4)_2S$-passivated NCs dissolved in DMF; the underlying interdigitated electrode pattern is visible. The scale bar is 10 μm.

resulted in an exchange efficiency of 45%, due to reasons not clear at present, meaning that inks from our CIGS NCs are still contaminated with carbon-containing molecules. Nevertheless, we observed that the OLAM ligand exchange, even if partial, still positively affected the electrical transport properties in films of such NCs.

As indicated by the SEM images (background of Figure 5c), the S-capped NCs yielded a continuous film, free of large-scale cracks or voids (Figure S11 in the Supporting Information). In contrast, films prepared from OLAM-coated NCs were severely cracked (Figure S12 in the Supporting Information). The dark current and photocurrent versus the bias voltage (recorded at RT) of the film of S-capped NCs are plotted in Figure 5c and yielded a film resistance $R = U/I$ of $R_{pristine} = 25$ MΩ in the dark. By considering the channel cross section and length with $A = 200$ μm^2 and $L = 10$ μm, we obtain a resistivity of $\rho_{LE} = 50$ Ω·cm. We observed a photocurrent to dark current ratio of 1.3. We note that the small ratio is given by the relatively high dark current, with an absolute photocurrent of about 100 nA at 1 V for this device. The linear current/voltage dependence for the film of S-capped CIGS NCs was characteristic for an ohmic behavior. As we start from CuS (metallic) NCs, we could still have Cu-deficient CIGS, resulting in a strongly doped thin film, even though the plasmon resonance is no longer observed in the NIR. Consequently, the Fermi level could be close to the valence band, yielding an ohmic contact with the gold electrode. With the photovoltaic applications of the CIGS NC films in mind, besides the need to attain quantitative ligand exchange, further work should be aimed at reducing the dark current and concomitant ohmic behavior significantly, which could be achieved by tuning the band alignment at the metal contacts and by reduction of the possible contaminations that could lead to defect states. The preparation of these inks represents only a first step of the solar cell fabrication process, which will be followed by further processing (thermal annealing to melt the NCs, chalcogenization, etc.), with the aim to optimize the properties of the final bulk film.

4. CONCLUSIONS

In summary, we have reported a facile phosphine-free heating procedure for the synthesis of quaternary CIGS. By tailoring the precursor molar ratios, we could tune the composition of the resultant NCs over the whole range, from $CuInS_2$ to $CuGaS_2$. These NCs demonstrated composition-dependent optical absorption properties, with a band gap increase from 1.48 to 2.10 eV with increasing Ga content. By scaling up the amount of precursors 15-fold using the same synthesis scheme, gram-scale amounts of CIGS powders could be collected, which was facilitated by the high chemical yield of the synthesis (90%), while still maintaining control over the phase, composition, band gap energy, and particle size. Ligand exchange procedures could only partially replace the native surfactants on the surface of these NCs with sulfur ions, indicating that further improvements are required to prepare colloidal NC inks that are entirely carbon-free. High-quality films of partially exchanged NCs exhibited high conductivity (both in the dark and under illumination). Given the general approach in terms of precursors, solvents, and temperatures used, our strategy might be suitable for large-scale synthesis of nanomaterials for low-cost photovoltaics.

■ ASSOCIATED CONTENT

Supporting Information

TEM images, size distribution, absorbance spectra, and EDS and XPS analyses of aliquot samples collected at different temperatures from RT to 250 °C, TEM images and absorbance spectra of CIGS aliquots collected at 250 °C and at different reaction times, determination of the band gaps of CIGS with different compositions, TEM images, XRD, and size distributions of CIGS NCs synthesized at different temperatures for 30 min, and EDS spectrum and analysis and band gap determination of large-scale synthesized CIGS NCs (PDF). This material is available free of charge via the Internet at http://pubs.acs.org.

■ AUTHOR INFORMATION

Corresponding Author

*E-mail: liberato.manna@iit.it.

Present Address

[‖]E.D. and Y.X. contributed equally to this work.

Notes

The authors declare no competing financial interest.

■ ACKNOWLEDGMENTS

The research leading to these results has received funding from the European Union's Seventh Framework Programme FP7/2007-2013 under Grant Agreement Nos. 284486 (SCALENANO), PIEF-GA-2011-298022 (NIRPLANA), and 240111 (ERC Grant NANO-ARCH).

■ REFERENCES

(1) Gabor, A. M.; Tuttle, J. R.; Albin, D. S.; Contreras, M. A.; Noufi, R.; Hermann, A. M. *Appl. Phys. Lett.* **1994**, *65*, 198−200.
(2) Schmidtke, J. *Opt. Express* **2010**, *18*, A477−A486.
(3) Kemell, M.; Ritala, M.; Leskela, M. *Crit. Rev. Solid State Mater. Sci.* **2005**, *30*, 1−31.
(4) Shi, J. H.; Li, Z. Q.; Zhang, D. W.; Liu, Q. Q.; Sun, Z.; Huang, S. M. *Prog. Photovoltaics: Res. Appl.* **2011**, *19*, 160−164.
(5) Sang, B.; Adurodija, F.; Taylor, M.; Lim, A.; Taylor, J.; Chang, Y.; McWilliams, S.; Oswald, R.; Stanbery, B. J.; van Hest, M.; Nekuda, J.; Miedaner, A.; Curtis, C.; Leisch, J.; Ginley, D. *PVSC: 2008 33rd IEEE Photovoltaic Specialists Conference*; Institute of Electrical and Electronics Engineers (IEEE): New York, 2008; Vols. *1*−*4*, pp 661−664.
(6) Kaelin, M.; Rudmann, D.; Kurdesau, F.; Zogg, H.; Meyer, T.; Tiwari, A. N. *Thin Solid Films* **2005**, *480*−*481*, 486−490.
(7) Mitzi, D. B.; Yuan, M.; Liu, W.; Kellock, A. J.; Chey, S. J.; Gignac, L.; Schrott, A. G. *Thin Solid Films* **2009**, *517*, 2158−2162.
(8) Todorov, T.; Gunawan, O.; Chey, S. J.; de Monsabert, T. G.; Prabhakar, A.; Mitzi, D. B. *Thin Solid Films* **2011**, *519*, 7378−7381.
(9) Hersh, P. A.; Curtis, C. J.; van Hest, M.; Habas, S. E.; Miedaner, A.; Ginley, D. S.; Stanbery, B. J.; Eldada, L. *35th IEEE Photovoltaic Specialists Conference*; Institute of Electrical and Electronics Engineers (IEEE): New York, 2010; pp 3430−3431.
(10) Panthani, M. G.; Akhavan, V.; Goodfellow, B.; Schmidtke, J. P.; Dunn, L.; Dodabalapur, A.; Barbara, P. F.; Korgel, B. A. *J. Am. Chem. Soc.* **2008**, *130*, 16770−16777.
(11) Gur, I.; Fromer, N. A.; Geier, M. L.; Alivisatos, A. P. *Science* **2005**, *310*, 462−465.
(12) Mitzi, D. B.; Yuan, M.; Liu, W.; Kellock, A. J.; Chey, S. J.; Deline, V.; Schrott, A. G. *Adv. Mater.* **2008**, *20*, 3657−3662.
(13) Wu, Y.; Wadia, C.; Ma, W.; Sadtler, B.; Alivisatos, A. P. *Nano Lett.* **2008**, *8*, 2551−2555.
(14) Luther, J. M.; Law, M.; Beard, M. C.; Song, Q.; Reese, M. O.; Ellingson, R. J.; Nozik, A. J. *Nano Lett.* **2008**, *8*, 3488−3492.
(15) Huynh, W. U.; Dittmer, J. J.; Alivisatos, A. P. *Science* **2002**, *295*, 2425−2427.
(16) Choi, J. J.; Lim, Y.-F.; Santiago-Berrios, M. E. B.; Oh, M.; Hyun, B.-R.; Sun, L.; Bartnik, A. C.; Goedhart, A.; Malliaras, G. G.; Abruña, H. D.; Wise, F. W.; Hanrath, T. *Nano Lett.* **2009**, *9*, 3749−3755.
(17) Kruszynska, M.; Borchert, H.; Parisi, J.; Kolny-Olesiak, J. *J. Am. Chem. Soc.* **2010**, *132*, 15976−15986.
(18) Connor, S. T.; Hsu, C.-M.; Weil, B. D.; Aloni, S.; Cui, Y. *J. Am. Chem. Soc.* **2009**, *131*, 4962−4966.
(19) Jiang, C.; Lee, J.-S.; Talapin, D. V. *J. Am. Chem. Soc.* **2012**, *134*, 5010−5013.
(20) Wang, J.-J.; Wang, Y.-Q.; Cao, F.-F.; Guo, Y.-G.; Wan, L.-J. *J. Am. Chem. Soc.* **2010**, *132*, 12218−12221.
(21) Tang, J.; Hinds, S.; Kelley, S. O.; Sargent, E. H. *Chem. Mater.* **2008**, *20*, 6906−6910.
(22) de Kergommeaux, A.; Fiore, A.; Faure-Vincent, J.; Chandezon, F.; Pron, A.; de Bettignies, R.; Reiss, P. *Mater. Chem. Phys.* **2012**, *136*, 877−882.
(23) Wang, Y.-H. A.; Zhang, X.; Bao, N.; Lin, B.; Gupta, A. *J. Am. Chem. Soc.* **2011**, *133*, 11072−11075.
(24) Guo, Q.; Ford, G. M.; Hillhouse, H. W.; Agrawal, R. *Nano Lett.* **2009**, *9*, 3060−3065.
(25) Norako, M. E.; Greaney, M. J.; Brutchey, R. L. *J. Am. Chem. Soc.* **2012**, *134*, 23−26.
(26) Yang, H.; Jauregui, L. A.; Zhang, G.; Chen, Y. P.; Wu, Y. *Nano Lett.* **2012**, *12*, 540−545.
(27) Shavel, A.; Cadavid, D.; Ibáñez, M.; Carrete, A.; Cabot, A. *J. Am. Chem. Soc.* **2012**, *134*, 1438−1441.
(28) Tsuji, I.; Kato, H.; Kobayashi, H.; Kudo, A. *J. Phys. Chem. B* **2005**, *109*, 7323−7329.
(29) Li, L.; Pandey, A.; Werder, D. J.; Khanal, B. P.; Pietryga, J. M.; Klimov, V. I. *J. Am. Chem. Soc.* **2011**, *133*, 1176−1179.
(30) Sun, C.; Westover, R. D.; Long, G.; Bajracharya, C.; Harris, J. D.; Punnoose, A.; Rodriguez, R. G.; Pak, J. J. *Int. J. Chem. Eng.* **2011**, *2011*, 545234.
(31) Nag, A.; Kovalenko, M. V.; Lee, J.-S.; Liu, W.; Spokoyny, B.; Talapin, D. V. *J. Am. Chem. Soc.* **2011**, *133*, 10612−10620.
(32) Moreels, I.; Fritzinger, B.; Martins, J. C.; Hens, Z. *J. Am. Chem. Soc.* **2008**, *130*, 15081−15086.
(33) Zhao, Y.; Pan, H.; Lou, Y.; Qiu, X.; Zhu, J.; Burda, C. *J. Am. Chem. Soc.* **2009**, *131*, 4253−4261.
(34) Kundu, M.; Hasegawa, T.; Terabe, K.; Yamamoto, K.; Aono, M. *Sci. Technol. Adv. Mater.* **2008**, *9*, 035011.
(35) Goh, S. W.; Buckley, A. N.; Lamb, R. N.; Rosenberg, R. A.; Moran, D. *Geochim. Cosmochim. Acta* **2006**, *70*, 2210−2228.
(36) Naumkin, A. V.; Kraut-Vass, A.; Gaarenstroom, S. W.; Powell, C. J. NIST X-ray Photoelectron Spectroscopy Database, NIST Standard Reference Database 20, version 4.1, 2012. http://srdata.nist.gov/xps/ (accessed March 25, 2013).
(37) Jehl, Z.; Bouttemy, M.; Lincot, D.; Guillemoles, J. F.; Gerard, I.; Etcheberry, A.; Voorwinden, G.; Powalla, M.; Naghavi, N. *J. Appl. Phys.* **2012**, *111*, 114509−114516.
(38) Chang, J.-Y.; Cheng, C.-Y. *Chem. Commun.* **2011**, *47*, 9089−9091.
(39) Choi, S.-H.; Kim, E.-G.; Hyeon, T. *J. Am. Chem. Soc.* **2006**, *128*, 2520−2521.
(40) Qi, Y.; Liu, Q.; Tang, K.; Liang, Z.; Ren, Z.; Liu, X. *J. Phys. Chem. C* **2009**, *113*, 3939−3944.